NANO MICRO small



# Adverse Effects of Titanium Dioxide Nanoparticles on Human Dermal Fibroblasts and How to Protect Cells

*Zhi Pan, Wilson Lee, Lenny Slutsky, Richard A. F. Clark, Nadine Pernodet, and Miriam H. Rafailovich**

*The effects of exposure of human dermal fibroblasts to rutile and anatase $TiO_2$ nanoparticles are reported. These particles can impair cell function, with the latter being more potent at producing damage. The exposure to nanoparticles decreases cell area, cell proliferation, mobility, and ability to contract collagen. Individual particles are shown to penetrate easily through the cell membrane in the absence of endocytosis, while some endocytosis is observed for larger particle clusters. Once inside, the particles are sequestered in vesicles, which continue to fill up with increasing incubation time till they rupture. Particles coated with a dense grafted polymer brush are also tested, and, using flow cytometry, are shown to prevent adherence to the cell membrane and hence penetration of the cell, which effectively decreases reactive oxygen species (ROS) formation and protects cells, even in the absence of light exposure. Considering the broad applications of these nanoparticles in personal health care products, the functionalized polymer coating can potentially play an important role in protecting cells and tissue from damage.*

**Keywords:**
- cells
- cytotoxicity
- fibroblasts
- nanoparticles
- titanium dioxide

## 1. Introduction

Due to their unique size-related properties such as high quantum yield and large surface area to volume ratio, nanomaterials have shown emerging applications in electronics, biology, and medicine.[1] As a result, the biomedical use of nanomaterials is being explored in broad areas such as nanoimaging, drug delivery, biosensors, and cancer phototherapy.[2] However, size effects of nanomaterials may also cause higher toxicity because of their larger surface area, enhanced chemical reactivity, and easier cell penetration.[3] Recently, it has been shown that scale alone could have adverse effects on cell function.[4] Pernodet et al.[5] have shown that the presence of Au particles, which are considered an inert material for living cells, was sufficient to induce aberrant actin formation and interfere with cell migration. Hence it is to be expected that when the particles are chemically active, that size effects can also exacerbate the adverse effects. Actually, for those materials possessing nanostructure-dependent properties, such as chemical, mechanical, electrical, optical, magnetic, and biological properties, which make them more important for commercial use, the same properties may potentially lead to adverse effects that differ from the bulk properties of these materials. Therefore, the safety issue of nanomaterials, especially those used for consumer applications, has attracted increasing attention.[6]

Here, we focused on $TiO_2$, which is a naturally occurring mineral and known to be biologically inert and nontoxic at the microscale in both humans and animals.[7] $TiO_2$ has been widely used in industry as an additive for products ranging from paint, to food colorant, to cosmetics and drugs. The most common use of $TiO_2$ is as an additive in cosmetics where its high absorbance for UV radiation is used to increase the sun

[*] Prof. M. H. Rafailovich, Z. Pan, Dr. W. Lee, L. Slutsky, Prof. N. Pernodet
Materials Science and Engineering
State University of New York at Stony Brook
Stony Brook, NY 11794 (USA)
E-mail: miriam.rafailovich@sunysb.edu
Prof. R. A. F. Clark
Biomedical Engineering, Dermatology and Medicine
State University of New York at Stony Brook
Stony Brook, NY 11794 (USA)

DOI: 10.1002/smll.200800798

protection factors (SPFs) of sunscreens. The same property also makes $TiO_2$ an important component for food packaging where it is added to prevent damage from UV radiation and increase shelf life. However, once it absorbs UV light, $TiO_2$, as a well-known photocatalyst, also catalyzes the generation of reaction oxygen species (ROS). This property makes $TiO_2$ a favorite component for antibacterial applications,[8] as well a major component in solar power cells, where sunlight is converted to electricity.[9] As pointed out by Dunford et al.,[10] the same property can also make $TiO_2$ a potentially hazardous material since ROS products in turn are known to cause genetic damage and other adverse effects in living tissues.[11] The ability of $TiO_2$ to photocatalyze the production of ROS products is further enhanced when the particles are ground to nanometer dimensions, thereby increasing the surface area and the electron flux. For example, it was shown that they can cause inflammatory reactions in both animals and humans when ground into particles smaller than 20 nm.[12]

Many studies reported that cells cultured in the presence of $TiO_2$ nanoparticles showed a dramatic decrease in growth rate with exposure to concentrations larger than 0.1 mg $mL^{-1}$.[13] Most of these reports directly correlated the cytotoxicity of $TiO_2$ nanoparticles to induced oxidative damage.[14] But, since most of the experiments were conducted in the dark, the source of the oxidative process was not immediately apparent. In order to understand the mechanism in more detail, and especially to determine if something could be done to prevent the damage, we have performed in vitro experiments with different types of $TiO_2$ nanoparticles. And since most of the previous experiments were performed with transformed cell lines that have been shown to be more sensitive to nanoparticle damage than normal primary cells, we chose to study the phenomena with human dermal fibroblasts from primary cultures. The skin is the primary barrier against contact penetration in cosmetic products and thus it was important to understand the effects that are specific to these cells with different particles that are commonly encountered in cosmetic formulations. In particular, Lee et al. recently showed that it was possible to graft a dense polymer coating onto the $TiO_2$ particles that can trap the photoelectrons and suppress ROS production.[15] We therefore performed a detailed study in order to determine how these particles also behaved in vitro when they came in contact with live cell cultures.

## 2. Results and Discussion

### 2.1. $TiO_2$ Nanoparticle Characterization

In Figure 1 we show scanning electron microscopy (SEM) and transmission electron microscopy (TEM) images of the $TiO_2$ particles that we used. The uncoated rutile particles tend to agglomerate into large spheres several micrometers in diameter. From Figure 1a it is clear that the spheres are composed of smaller particles. In order to image them directly, we dispersed the spheres in ethanol and then spread a droplet of the solution onto a carbon-coated TEM grid. The TEM image is shown in Figure 1b, where we see that the particles are oblate, but of uniform size and shape. The average width of the particles is $15.0 \pm 3.5$ nm, and they are elongated with an aspect ratio of $\approx$3.92. In commercial products, the aggregates are difficult to compound in formulations, and hence micrometer-sized talc is frequently added to act as a dispersant. The talc particles are hard and angular, which allows them to break the aggregates and disperse the particles more uniformly. This can be seen in the SEM image of anatase $TiO_2$ particles (Figure 1c). Figure 1d is the TEM image of these anatase $TiO_2$ particles with talc, where it is clearer that they have different shapes from rutile particles and much larger sizes, $200 \pm 13$ nm. The crystallographic structures of these two different types of $TiO_2$ particles were confirmed by X-ray diffraction (XRD).

These particles, in either rutile or anatase phase, are commonly used in consumer products. Hence in this paper, we compared both ultra-fine rutile $TiO_2$ (US Cosmetics) nanoparticles and dispersed anatase $TiO_2$ (US Cosmetics) nanoparticles, both of which are regarded as a biocompatible material in the absence of photoactivation. Although it is generally thought that smaller nanoparticles penetrate cells more easily and induce higher damages, we found that phase is a more crucial factor than size or shape, which is consistent with previous reports.[13]

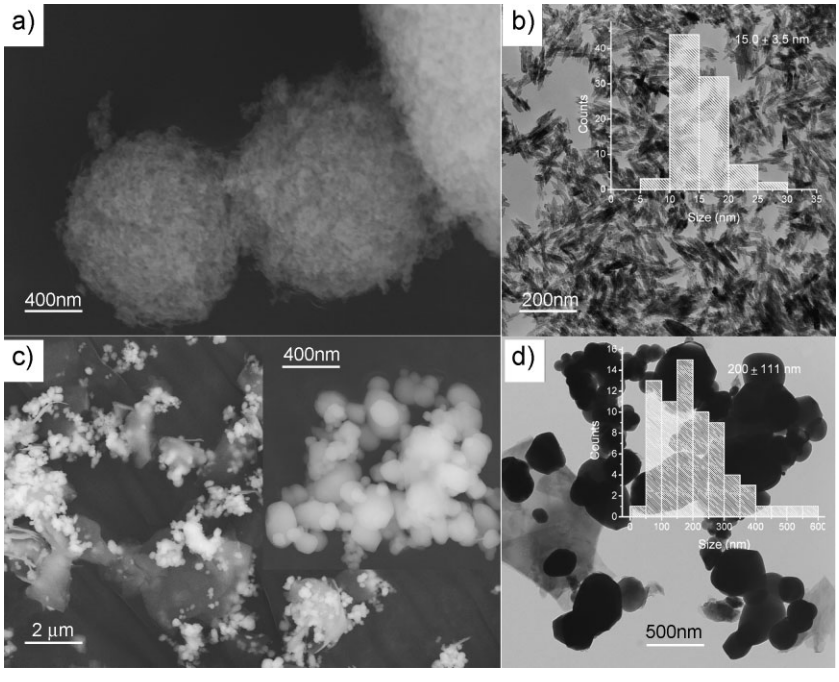


**Figure 1.** Microscopy images of different types of $TiO_2$ particles used in this study. a) SEM images of microscale clusters of rutile $TiO_2$ particles. b) TEM images of rutile $TiO_2$ nanoparticles and particle size distribution. c) SEM images of clusters of anatase $TiO_2$ particles with talc particles used as dispersant (inset: magnified image of an anatase cluster showing individual particles). d) TEM images of anatase $TiO_2$ nanoparticles and particle size distribution.

  

NANO MICRO small

In this study, we also noticed that the $TiO_2$ particles are naturally fluorescent with a broad band excitation in the range from UV to optical. The fluorescence spectrum is also very broad with no apparent peak in intensity in the observed region. On one hand, the effect can perturb studies where one is counting specific florescence from a particular stain, such as measurements detecting apoptosis, metabolism, and ROS. On the other hand, if we do not use staining, this can be a useful tool for detecting nanoparticles associated with cells.

### 2.2. Rutile $TiO_2$ Nanoparticles

In order to determine the effects of nanoparticle exposure on cell conformation we incubated human dermal fibroblasts with the rutile particles shown in Figure 1a and b. The confocal images of cells with stained actin (green) and nuclei (red) are shown in Figure 2a, from which we can see that after 6 days of incubation, the introduction of rutile $TiO_2$ particles caused a large decrease in the cell area as compared to the control sample. Closer examination of the image also indicates that the morphology of the cells is affected. The control cells are triangulated and well-spread on the surface, while the cells exposed to $TiO_2$ have become elongated and appear to detach from the surface. This is also shown graphically in Figure 2b where we plot the cell area averaged over several hundred cells that were incubated with 0.4 and 0.8 mg $mL^{-1}$ of particles for 6 days. In Figure 2b we can see that the cell area of the experimental samples is on average 1/4 and 1/5, respectively, that of the control sample incubated at the same time without particles. In Figure 2a, we can also see that in analogy with the findings of Pernodet et al. on the same cell model,[5] the decrease in area is also associated with a change in the actin fibers, where they become thinner and less extended.

Since actin is implicated in many cell functions and behaviors, such as cell division, we also measured the proliferation at these particle concentrations. The cell numbers after 6 days of incubation are plotted in Figure 2b. From the figure we can see that the cell counts are drastically reduced, and the cells, although still alive, have nearly stopped dividing. Most previous toxicity studies have focused on cell death,[4] but here we show that for low concentration the cells can survive, but the question of their ability to perform essential functions arises.

Dermal fibroblasts play a central role in the wound healing process. In the initial process, they migrate into the wound site and tissue repair begins when they contract the collagen fibers so that keratinocytes can differentiate and form the subsequent layers of skin tissue. These functions are composed of two separate processes: cell migration and collagen contraction, both of which depend on the ability of the cells to exert traction forces on the substrate. In order to study whether nanoparticles influence cell function, we first exposed cells to 0.4 mg $mL^{-1}$ $TiO_2$ nanoparticles for 2 days, and then compared their functions with normal control cells. We first measured the effect on traction forces exerted by the cells using techniques described previously.[16] We used a synthetic hydrogel composed of crosslinked, functionalized hyaluronic acid (HA) and fibronectin-functional domains (FNfds) as the flexible substrate impregnated with fluorescent beads. The digital image speckle correlation (DISC) technique combined with the finite element method (FEM) was then used to measure the traction stress intensity and distribution on the surfaces. The results are shown in Figure 3a for a representative cell. We can see that in the absence of nanoparticles, the cells are well-spread on the hydrogel, and robust traction forces are exerted along the periphery. The hydrogel used here was relatively stiff, and good cell adhesion and triangulation was previously reported.[17] When the nanoparticles are added, even though the cells prefer these surfaces, the cell area is reduced and the cells become elongated. Elongation can also be associated with cell migration. This was previously described by Ghosh et al. when cells were plated on softer surfaces where large traction forces only appeared behind the leading edge and cells migrated faster.[16] Here we see that despite the elongated appearance, only weak traction forces are exerted.

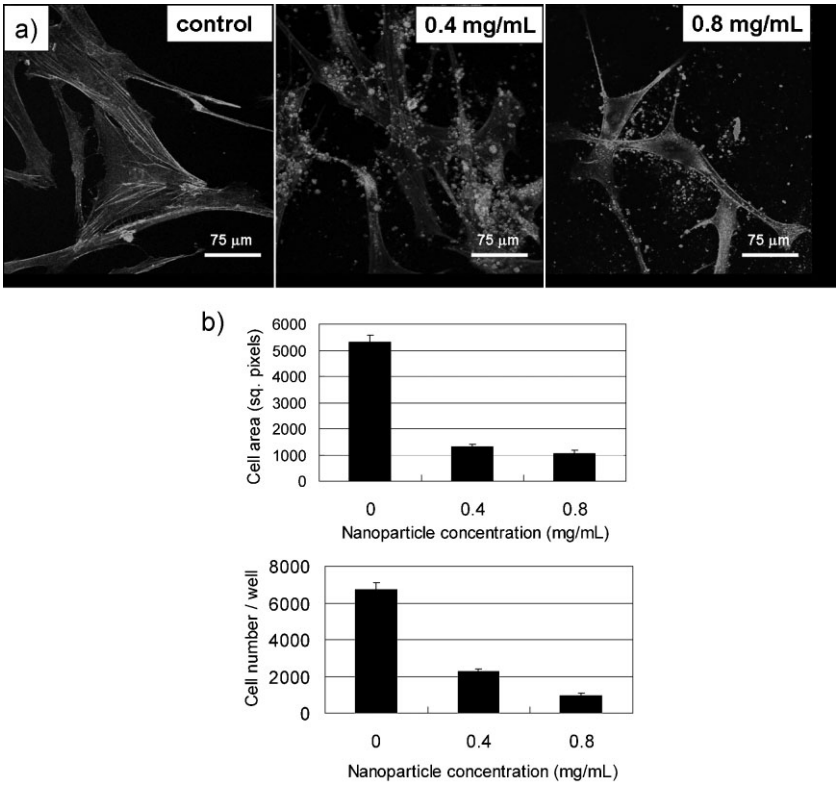


**Figure 2.** a) Confocal images of human dermal fibroblasts incubated for 6 days with different concentrations of rutile $TiO_2$ nanoparticles. b) Cell area and number as a function of nanoparticle concentration.

Cell migration was then measured in a separate set of experiments where an agarose droplet cell migration assay was

  

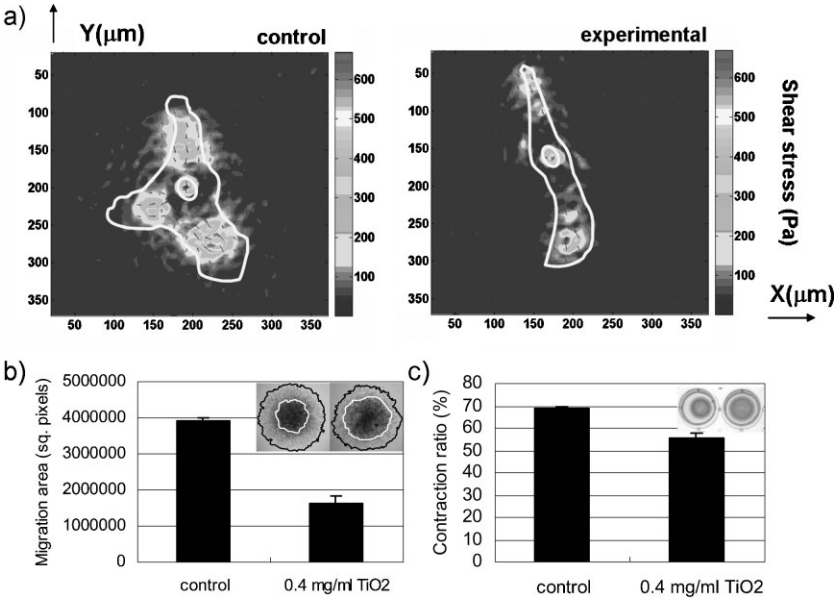


**Figure 3.** Cells were incubated with 0.4 mg $mL^{-1}$ rutile $TiO_2$ nanoparticles for 2 days and then assayed for the following functions: a) traction stresses exerted by cells on a hydrogel after 6 h of incubation; b) cell migration area out of an agarose droplet after 18 h of incubation; and c) contraction of collagen gels after 4 h of incubation.

done. Here we defined the migration area as the difference between the total area that cells covered after 18 h of migration and the area of the agarose droplet. The results are shown in Figure 3b. In the inset phase images, the black rings delineate the periphery of the migrating circles of cells and the white rings show the area of agarose droplets, where we can clearly see that the migration is far smaller for cells exposed to 0.4 mg $mL^{-1}$ $TiO_2$ than for the unexposed cells. Using the migration area to evaluate the cell mobility, we can see that the $TiO_2$ exposure reduced migration by ≈59%.

The ability of cells to contract the collagen matrix was also studied. The same number of normal cells and cells incubated with 0.4 mg $mL^{-1}$ $TiO_2$ particles were cultured in collagen gels for 4 h. The optical images of the gels are shown in the inset of Figure 3c, where we can clearly see that the collagen gels contacted by the normal cells are significantly smaller than those contracted by cells exposed to $TiO_2$. The collagen contraction ratios averaged over three samples are plotted in Figure 3c. The contraction of cells exposed to $TiO_2$ was less than 80% of the control sample.

Since the $TiO_2$ particles can be excited with 488 nm radiation and their emission spectrum is wide, the particles are also apparent in the confocal microscope images, especially those obtained using Hg lamp florescence. Due to the resolution of microscopy, the fluorescence observed is from large particle clusters. In order to visualize how the particles entered the cell and where they were sequestered, we performed electron microscopy on cells incubated with 0.4 mg $mL^{-1}$ rutile $TiO_2$ nanoparticles. We first imaged cells incubated with the $TiO_2$ nanoparticles for 2 days, the same time scale used for migration and contraction studies. A typical image is shown in Figure 4a. In these images, we can clearly see the $TiO_2$ particles, which are more electron dense than the surrounding cell environment. After 2 days, even though the cells seem to have ingested a relatively large amount of particles, we know from the previous experiments that they have still retained the ability to perform most functions. Most of the particles seem to be confined inside vesicles that are distributed across the cytoplasm, but which do not cross into the nucleus. A higher magnification image of the vesicles was also obtained and is shown in Figure 4b. Here we see the particles that comprise the clusters surrounded by the vesicle membrane. In a previous study, Pernodet et al. also showed Au nanoparticles capsulated in single vesicles of dermal fibroblasts.[5] In that case, the vesicles were only partially filled with particles and the membranes of the vesicles were intact. Here it appears that many more particles are stuffed into each vesicle, thereby possibly leading to rupture. The boundary with the nuclear membrane is also visible in Figure 4b. Here we see that one of vesicles that is close to the nucleus does not have an intact enclosure, and the particles have begun to leak out. Several individual particles shown in the circle might be able to cross the nuclear membrane. Another instance is shown in Figure 4c, where we can see a vesicle containing a very large cluster of particles impinging upon the nucleus. The vesicle membrane surrounding the cluster appears ruptured; in the upper corner a segment of particles has pierced through the membrane, and in the back portion facing away from the nucleus the membrane is completely frayed. The nuclear membrane is distorted, but remains distinct from the vesicle membrane and is intact (dashed line). A small particle cluster is seen to have become lodged inside the membrane (indicated by an arrow), but has not penetrated into the nucleus.

In order to determine how the particles entered the cell, we also performed a series of TEM cross sections corresponding to a time-sequence incubation (Figure 5a). We can see that

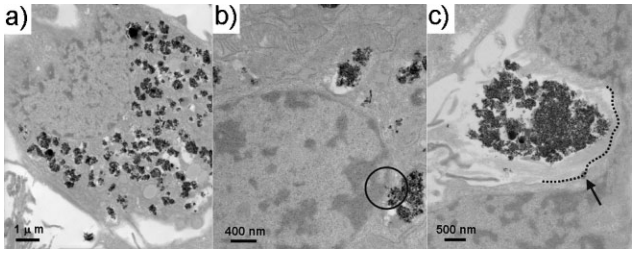


**Figure 4.** TEM images of cells incubated with 0.4 mg $mL^{-1}$ rutile $TiO_2$ nanoparticles for 2 days. a) A typical cell with nanoparticle clusters confined in vesicles. b) Vesicles filled with nanoparticles (the red circle shows individual particles leaking out from the vesicles). c) A vesicle with a ruptured membrane (the dashed shows the nuclear membrane and the arrow shows a small particle cluster lodged inside the nuclear membrane).

  

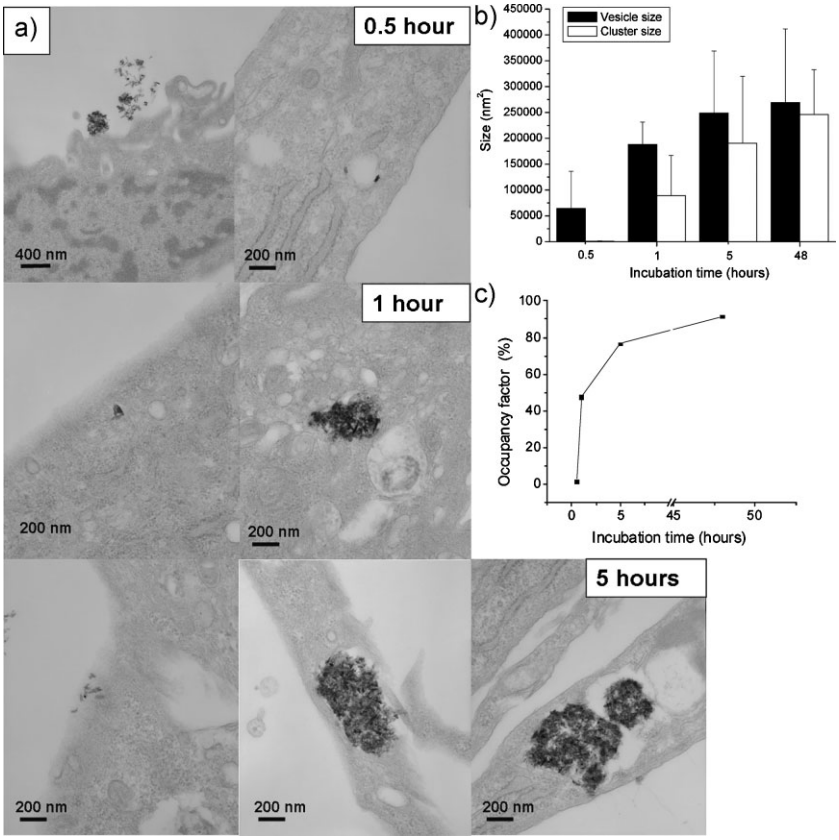


**Figure 5.** A time sequence study of cells incubated with 0.4 mg $mL^{-1}$ rutile $TiO_2$ nanoparticles. a) TEM images. b) Vesicles size and particle cluster size. c) Occupancy factor as a function of incubation time.

after 30 min, some particles are attached to the cell membrane, but very few have penetrated inside the cells. A closer examination of the particles on the membrane indicates that some are lodged on the membrane, but no evidence of endocytosis is observed for the isolated particles. Larger clusters can also be seen on the membrane, but no evidence of penetration as clusters is observed. A closer examination of the images shows individual particles are already lodged inside large otherwise empty vesicles. In Figure 5b we plot the mean size of both vesicles and clusters as a function of incubation time. We find that at 30 min, the size of the vesicles is fairly uniform with a mean diameter of ≈286 nm, which is much larger than the individual particle size. After 1 h, larger clusters are seen to form inside the vesicles, and individual particles are observed at the membrane. With times up to 5 h, the amount of individual particles at the membrane increases, and clusters are also observed with the indented cell membrane, which is in the process of endocytosis. At the same time, the size of the clusters in the vesicle increases dramatically. From Figure 5b we can see that the cluster size approaches ≈77% of the mean vesicle size after 5 h, and both the vesicle size and the cluster size do not increase significantly after that time. We can therefore define an occupancy factor as the ratio of cluster to vesicle size. We then plot occupancy factor versus incubation time in Figure 5c where we see that it increases rapidly in the first 5 h and then levels off in the next 43 h. In this case, as more particles enter the cells, more vesicles are created and then filled. The cluster size is limited by the vesicle size. Any further increase in cluster size probably leads to the rupture of the vesicle. This can be seen in the TEM images of the particle clusters shown in Figure 4c, where the size of the vesicle filled with clusters is almost ten times the average size.

## 2.3. Anatase $TiO_2$ Nanoparticles

Anatase $TiO_2$ is known to be even more photoactive than rutile. In Figure 6a we show confocal images of cells incubated with anatase $TiO_2$ particles at different concentrations for 3 days. Compared with Figure 2 we can see that anatase particles with even lower concentrations and shorter incubation times can produce far more damage to the cells than rutile particles. A closer examination indicated that even the cells incubated with 0.1 mg $mL^{-1}$ of anatase particles had broken actin fibers and nanoparticles surrounding the nuclear membrane. Cells incubated at the higher concentrations had nearly no visible actin fibers, and the membranes appeared to have ruptured. To further confirm that the damage to the actin cytoskeleton was caused by anatase $TiO_2$ nanoparticles rather than microscale talc particles, another control sample with an equal amount of talc was examined, where we can see that cells

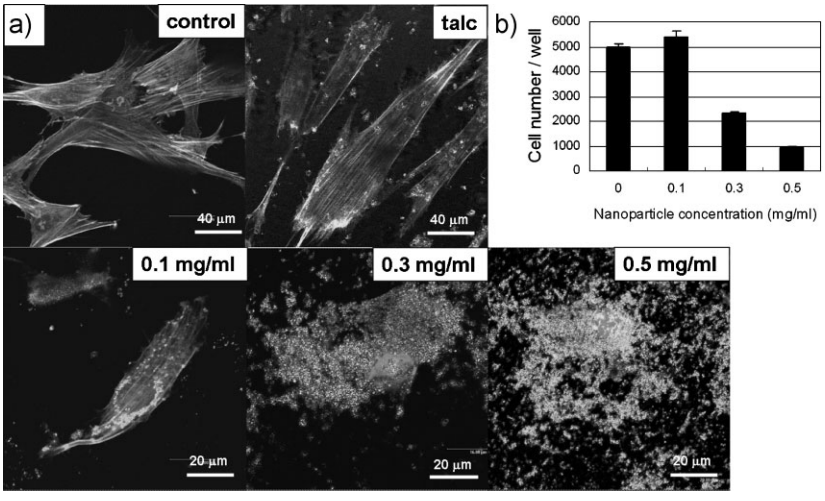


**Figure 6.** a) Confocal images of cells incubated with different concentrations of anatase $TiO_2$ nanoparticles for 3 days. b) Cell number as a function of nanoparticle concentration.

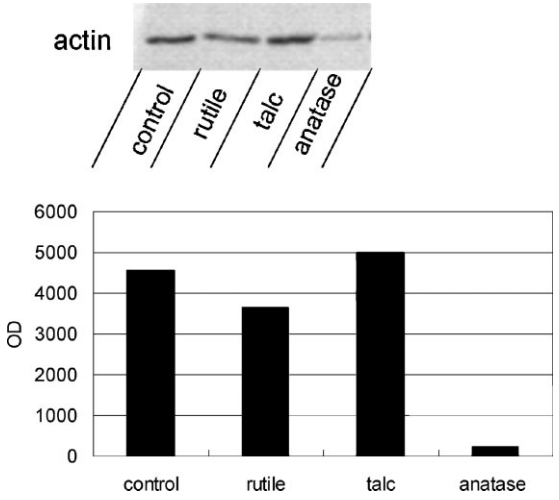


**Figure 7.** Western blot results of actin from the same number of cells incubated with 0.4 mg $mL^{-1}$ rutile or anatase $TiO_2$ nanoparticles for 2 days compared with those exposed to no particles or just talc particles at the same concentration.

cultured in media with talc still grew well after 3 days and showed clear and strong actin fibers. These results are consistent with the survival cell number after being cultured for 7 days in the presence of anatase $TiO_2$ nanoparticles at different concentrations. As shown in the bar graph of Figure 6b, only cells incubated with 0.1 mg $mL^{-1}$ or less survived and were able to proliferate. Cells cultured with a concentration of 0.3 mg $mL^{-1}$ or higher failed to grow. Cell numbers were significantly decreased after exposure to high concentrations of anatase $TiO_2$ nanoparticles. The dramatic damage induced by anatase $TiO_2$ nanoparticles to actin was confirmed by Western blot. Compared to the adverse influence of rutile particles, anatase particles show a dramatic effect on the cell actin after 2 days of incubation (Figure 7), which would severely impair cell function.

Figure 8 shows TEM images of microtomed sections from cells exposed to 0.4 mg $mL^{-1}$ anatase $TiO_2$ nanoparticles. From Figure 8a we can see that the anatase particles caused huge holes to form in the cell cytoplasm, which may be the remnants of vesicles that were filled with particles. Although more damage was found outside of the nuclei, we also noticed some vesiculated nuclei (Figure 8b). This raises more issues, such as whether these nanoparticles could directly harm DNA molecules and induce further damage at the gene level. Previous studies about the effects of $TiO_2$ nanoparticles on DNA have already shown that DNA would be partially decomposed when exposed to UV radiation.[18] Here, the TEM images confirmed that this phenomenon cannot be neglected, because it is possible for nanoparticles to get into the nuclei of normal tissue cells under certain conditions.

## 2.4. Coated $TiO_2$ Nanoparticles

The first step in the penetration process appears to be adhesion of the

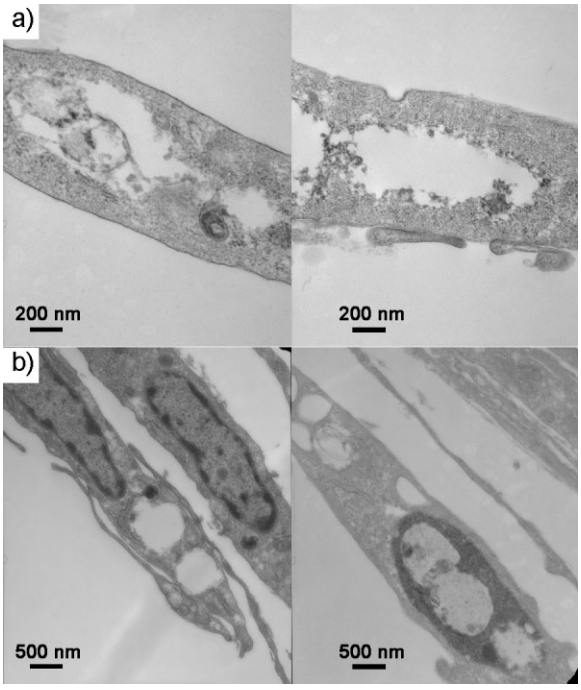


**Figure 8.** TEM images of cells incubated with 0.4 mg $mL^{-1}$ anatase $TiO_2$ nanoparticles for 2 days. a) Typical cells with huge holes induced by anatase particles. b) Most damage is distributed in the cytoplasm (left) and some vesiculated nuclei are also observed (right).

particles to the cell membrane. Hence we proposed that if the adhesion mechanism was somehow impeded, the penetration of the particles into the cells would be greatly reduced. Lee et al. have recently shown that it was possible to chemically graft a densely charged polymer layer onto the $TiO_2$ particles using sonochemical methods.[15] This layer was able to trap electrons emitted by the particles and form a dense polymer brush with an approximate grafting density of one chain per 0.6 nm. It is known that extremely stretched brushes do not adhere to surfaces, since entropic hindrance prevents further distortion of the brush, resulting in hard core repulsion. We therefore postulated that this effect may also prevent the coated particles from adhering to the cell surface membranes.

In order to probe this hypothesis, we first coated the rutile $TiO_2$ using the technique of Lee et al.[15] The SEM and TEM micrographs of coated rutile $TiO_2$ nanoparticles are shown in

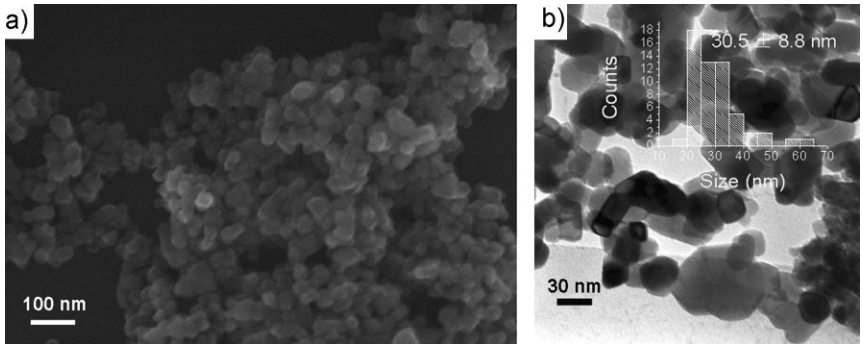


**Figure 9.** Microscopy images of coated rutile $TiO_2$ particles. SEM images (a) and TEM images (b) of coated rutile $TiO_2$ nanoparticles and particle size distribution.

NANO MICRO small

Figure 9. We then added different concentrations of the coated rutile $TiO_2$ nanoparticles to cell culture media and compared the data with that obtained from samples containing equal concentrations of the non-coated rutile particles. From Figure 2b we have shown that cells incubated with non-coated rutile $TiO_2$ particles have a much slower proliferation rate than the control sample. Here, cells incubated with coated particles are almost indistinguishable from the control samples for all times. In Figure 10a, cell counts after 11 days of incubation are still comparable to the control. Corresponding Hg lamp fluorescent images of the cells demonstrate particles in the media, but they do not appear to be in or on the cells (Figure 10b).

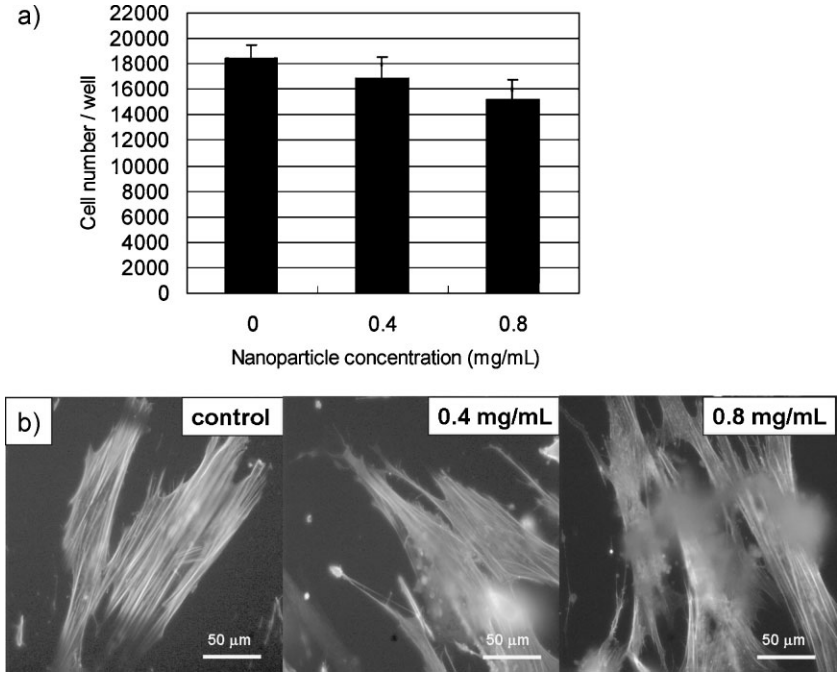


**Figure 10.** a) Cell numbers after being incubated with different concentrations of coated $TiO_2$ nanoparticles for 11 days. b) Hg lamp fluorescent images of cells incubated with coated $TiO_2$ nanoparticles.

Another method to compare the amount of $TiO_2$ particles adhered to the cells is flow cytometry. Since $TiO_2$ particles have a natural florescence, no additional staining is required. The results are shown in Figure 11 for cells incubated with 0.4 mg $mL^{-1}$ rutile, anatase, and coated rutile particles for 2 days. The largest florescence from all the particles was obtained with an excitation wavelength of 635 nm. Since the cells were washed many times to remove all the floating particles, the emission could only come from particles attached to the cells. In Figure 11, distinct peaks of high fluorescent intensity were observed with cells incubated with uncoated rutile or anatase particles, but not from cells incubated with coated $TiO_2$. These latter cells had an emission spectrum almost identical to the control, which consisted of cells that were not incubated with particles. If we assume that the average intensity is correlated to the number of particles associated with the cells, we can see that the anatase sample has the largest number. All these are consistent with optical micrographs of the samples prior to injection into flow cytometry (inset in Figure 11), where the particle uptake is significantly larger for cells incubated with anatase particles than with rutile ones, while nearly no uptake is observed for cells incubated with the coated rutile particles. Since we do not know the precise difference in intensity between the two phases of $TiO_2$ particles, we cannot at the moment use this technique to quantify the amount of particles in the cell. But compared with the control, which does not contain any particles and corresponds to the system background, we can still obtain a clear idea of the presence of different types of $TiO_2$ particles adhered to the cells. This is consistent with Figure 10 where we do not see coated $TiO_2$ particles inside the cells, and now we can also conclude that very few coated particles were adhered to the outside of the cells.

Since nanoparticles are also known to induce oxidative stress, we assayed the ROS production, using $H_2O_2$, of cells incubated under the same conditions as those used in the flow cytometry test. $H_2O_2$ produced by the cells incubated with

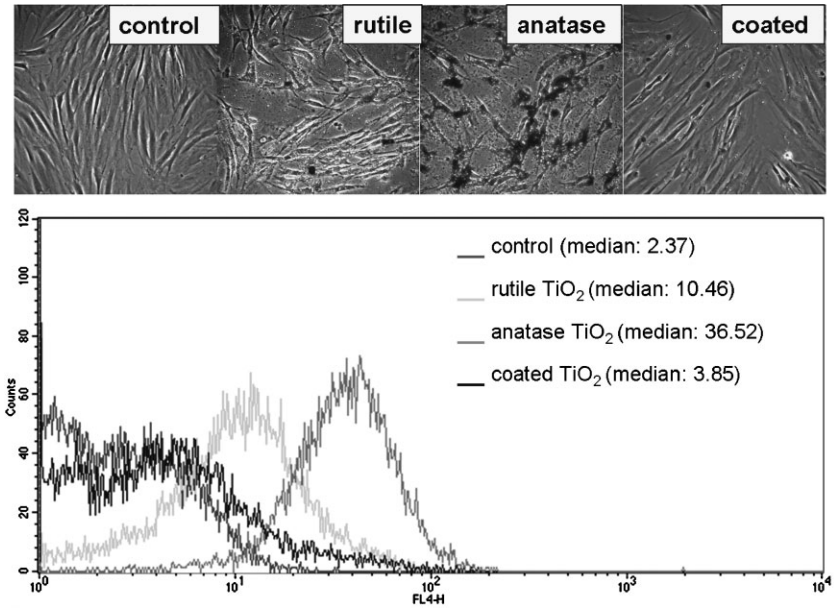


**Figure 11.** Flow cytometry results showing different particle uptake of cells after being incubated with 0.4 mg $mL^{-1}$ rutile, anatase, and coated $TiO_2$ nanoparticles for 2 days. The phase contrast images of cells with attached particles were taken prior to the flow cytometry analysis.

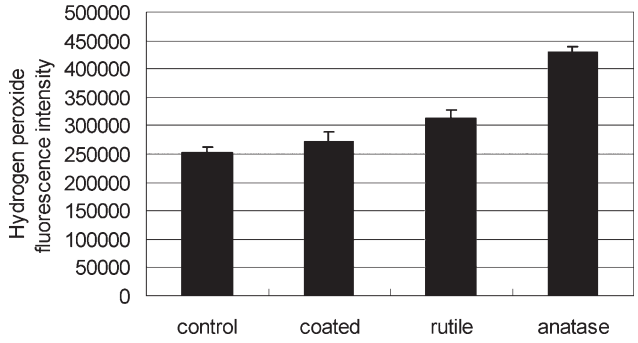


**Figure 12.** $H_2O_2$ generated and released by the cells incubated with 0.4 mg $mL^{-1}$ rutile, anatase, and coated $TiO_2$ nanoparticles for 2 days compared to the control cells exposed to no particles.

coated rutile particles was comparable to the control sample as shown in Figure 12. The $H_2O_2$ levels were significantly elevated by ≈24% and ≈70% for the cells incubated with rutile and anatase nanoparticles, respectively, which are consistent with the particle uptake and the damages induced by these particles. Since all the studies here are performed without light exposure, these results indicate that nanoparticle attachment and penetration may be the reason cells produce oxidative stress and induce ROS production.

## 3. Conclusion

In this study, we showed that both rutile and anatase $TiO_2$ nanoparticles impair cell function, with the latter being more potent at producing damage. Exposure to nanoparticles decreases cell area, proliferation, mobility, and ability to contract collagen. These $TiO_2$ nanoparticles can easily penetrate through cell membranes and are sequestered inside vesicles. In time vesicles fill up and eventually rupture. Particles that were coated with a polymer brush did not adhere to cell membranes and hence did not penetrate cells, which decreased ROS formation and thus allowed normal cell function. Considering the broad applications of these nanoparticles in personal health care products, the functionalized polymer coating can potentially play an important role in protecting cells and tissue from damage.

## 4. Experimental Section

*$TiO_2$ particle characterization:* Dry $TiO_2$ powder was used as a SEM sample to evaluate the particle size, shape, and suspended status. In order to image individual particles clearly, the powder was dispersed in ethanol and spread on a carbon-coated TEM grid. The crystallographic structures of these two different types of $TiO_2$ particles were confirmed with XRD. Additionally, different types of $TiO_2$ particles were suspended in phosphate buffer saline (PBS) and loaded in a 96-well dish prior to the fluorescence measurement, which was performed with a FLEXstation™ benchtop scanning fluorometer (Molecular Devices).

*Cell culture and function studies:* Primary dermal fibroblasts obtained from a 31-year-old Caucasian female (Clonetics) were used between passages 5 and 13. The cells were routinely cultured in full-Dulbecco's Modified Eagle Medium (DMEM) supplemented with fetal bovine serum (10%) and penicillin, streptomycin, and L-glutamine (P/S/G, 1%), in a 37 °C, 5% $CO_2$, 95% humidity incubator (Napco Scientific). $TiO_2$ media was prepared by dispersing the nanoparticles in the same full-DMEM at different concentrations. Before use, the $TiO_2$ media was sonicated for ≈30 min and stirred for at least 5 min to achieve a homogeneous distribution. The experimental samples were prepared by culturing cells in $TiO_2$ media at different concentrations for a certain incubation time, with the media changed every 2–3 days.

Immunofluorescence images of the cells were taken with a 40× oil lens on a Leica TCS SP2 laser scanning confocal microscope (Leica Microsystems) after the cells were stained by alexa fluor 488 phalloidin for actin and propidium iodide for nuclei. With MetaMorph software (Universal Imaging), the area of the cells on these confocal images can be readily measured.

For cell counting, cells were seeded in 24-well dishes with 2500 cells/well at the beginning. After being cultured with full-DMEM or $TiO_2$ media for a certain incubation time, cells were rinsed three times with PBS to remove any suspended particles and dead cells. Then they were detached with trypsin and counted with a hemacytometer. Each experimental group contained at least three replicates to obtain the average cell number under each condition.

Quantification of cellular traction forces was achieved with the DISC technique combined with FEM as previously reported.[16] After 2 days exposure to the media with or without $TiO_2$ nanoparticles, the experimental and control experimental cells were reseeded onto HA/FNfd hydrogels with fluorescent beads in DMEM and kept in a 37 °C incubator for 6 h. The images before and after cell detachment were recorded with a 63×, NA 0.9 water objective on a Leica TCS SP2 laser scanning confocal microscope (Leica Microsystems). The deformations were quantified with the DISC technique and the cellular traction stresses were calculated with FEM.

Cell migration was evaluated with an agarose droplet assay. The agarose gel was prepared by melting agarose stock solution (2% w/v) and diluting it with DMEM at a 1:9 ratio. Then the diluted agarose (0.2% w/v) was added to the cell pellets and the cells were resuspended to $1.5 \times 10^7$ cells $mL^{-1}$. Droplets (1.25 μL) of such cell suspension were carefully loaded on the prepared HA/FNfd hydrogel surfaces in a 24-well dish. After that, the whole dish was placed at 4 °C for 20 min to allow the agarose droplet to gel before DMEM (400 μL) with platelet derived growth factor (PDGF) (30 ng $mL^{-1}$) was added into each well. After 18 h of incubation at 37 °C, the cells were fixed with formaldehyde (3.7%), stained with crystal violet (0.1%), and rinsed three times with PBS for easy visualization under a stereomicroscope. To quantify cell migration, the area of agarose droplets and the area covered by the leading edges of the out-migrating cells were measured with SPOTCam software. The cell migration area was defined as the area of the outward cell migration minus the area of agarose droplets.

Collagen gel contraction is typically used to mimic the process of wound healing. Here, we measured the extent of gel contraction

  

NANO MICRO small

to evaluate the ability of cells to contract the collagen matrix. Cells were suspended in prepared collagen solution composed of purified collagen (1.8 mg $mL^{-1}$), bovine serum albumin (BSA, 2%), hFibronectin (30 μg $mL^{-1}$), and PDGF (100 ng $mL^{-1}$) in DMEM with P/S/G at $3 \times 10^5$ cells $mL^{-1}$. The cell/collagen gels (0.6 mL $well^{-1}$) were loaded into a BSA-coated 24-well dish. After preincubation for 2 h to gel the mixture, collagen gels were gently detached by slight tapping on the wells and DMEM (500 μL) with BSA (2%) and PDGF (100 ng $mL^{-1}$) were added. Then, after another 2 h of incubation, the phase images of the gels were taken and analyzed by measuring the gel size. The contracted ratio was defined as the ratio of the contracted area (which is the original gel size minus the final gel size) to the original gel size.

For Western blotting, whole cell lysate was prepared by scraping cells in lysis buffer with protease inhibitors and phenylmethylsulfonyl fluoride (PMSF), and then mixed with 4 × SDS-PAGE buffer composed of Tris (0.25 M, pH 6.8), sodium dodecyl sulfate (SDS, 8%), glycerol (40%), and bromophenol blue (0.02%) with dithiothreitol (DTT, 80 mM) at a volume ratio of 3:1. After the mixture was boiled at 100 °C for 3 min, the proteins from the same number of both control and experimental cells were separated by SDS-PAGE and electrophoretically transferred to a nitrocellulose membrane. Blots were probed with the anti-actin antibody, Act(C-11), goat polyconal IgG (Santa Cruz Biotechnology). The primary antibodies were then detected with the secondary antibodies, rabbit anti-goat IgG(H+L) (ImmunoPure Antibody, Pierce Biotechnology), followed by enhanced chemiluminescence (SuperSignal West Dura Extended Duration Substrate, Pierce Biotechnology). The picture of the bands was taken with a ChemiImager™ Ready camera (Alpha Innetech Corporation) and their densities were quantified with ChemiImager v5.5 (Alpha Innetech Corporation).

*TEM:* In order to monitor how $TiO_2$ nanoparticles penetrate cells and where they stay in cells, cells exposed to nanoparticles with different incubation times were fixed as follows and imaged with TEM. The fresh samples were rinsed three times with PBS and fixed for 30 min in modified Karnovsky fixative using glutaraldehyde (2.5% v/v) and paraformaldehyde (2% w/v) in cacodylate buffer (0.1 M, pH 7.2–7.4) with calcium chloride (2.5 mM). The samples were then rinsed three times with cacodylate wash buffer for ≈5 min. After that, the samples were post-fixed in osmic acid (2%) for 15 min and stained in a saturated aqueous solution of uranyl acetate for 15 min. The dehydration process was performed in a graded series of 30%, 50%, 70%, 95%, and twice in 100% ethanol, for 15 min each. Then the samples were infiltrated with a 50:50 mixture of 100% ethanol and Spurr's plastic. After discarding the mixture 1 h later, 100% Spurr's was added to infiltrate the cells for another 1 h. The samples were kept in a vacuum oven at 60 °C overnight after changing the Spurr's. Finally, the samples were cut into light-gold-colored ultrathin sections with a microtome and stained on the grid with uranyl acetate and lead oxide, each for 5 min. After being washed thoroughly with distilled water, TEM samples of cells were dried and then imaged under a Joel (model 1200EX) TEM. We analyzed the images by characterizing the penetration, distribution, and specific location of the nanoparticles, and by quantifying the size of vesicles and particle clusters at different time points for different types of nanoparticles.

*Particle coating:* Rutile $TiO_2$ nanoparticles were coated by chemically grafting dense antioxidant/anionic and hydrophobic polymer molecules directly onto the surface by a recently reported technique.[15] Briefly, antioxidant formed from grape seed extracts (oligomeric proanthocyanidins) and anionic polymer (poly[methyl-vinylether/maleic acid]) were mixed at a 1:1 ratio and dissolved in a 22:1 water/denatured ethanol solution using a lightening mixer at 25 °C. After the solution became homogeneous, a new mixture was prepared composed of the antioxidant/anionic polymer solution (30% w/w), deionized water (22% w/w), $TiO_2$ (43% w/w), and hydrophobic polymer (5% w/w, triethoxysilylethyl poly (dimethylsiloxyethyl dimethicone), Shin-Etu Chemical Co., Ltd.). The entire slurry was then sonicated for 30 min with medium intensity at 25 °C with an Ultrasonic probe (Sonicor Instrument Co.) at 20 KHz. In order to precipitate the particles and remove the excess polymers, the resultant mixture, which was a thick colloidal suspension, was then centrifuged for 15 min at 9000 rpm and washed with deionized water. The washing procedure was repeated three times in order to ensure that all unattached materials were removed. The product was then dried at 110 °C under vacuum for 16–20 h.

*Flow cytometry:* Both the control and the experimental cells were carefully rinsed more than three times to remove all the floating particles in the experimental media and detached with trypsin-ethylenediaminetetraacetic acid (EDTA). After stopping trypsin with full-DMEM, the cells were rinsed twice using DMEM with BSA (0.2%) for good separation. Then the cells were suspended and fixed in paraformaldehyde (1%) in PBS for 20 min. After being rinsed twice using PBS and resuspended in PBS at the concentration of $1 \times 10^6$ cells $mL^{-1}$, the sample solutions were ready for flow cytometry, which was performed with a BD FACSCalibur™ benchtop flow cytometer.

*Measurement of hydrogen peroxide:* The cellular level of $H_2O_2$ was measured with the aid of the fluorogenic probe, Amplex red, as described by Eu et al. with certain modifications.[19] Briefly, both the control and experimental cells exposed to different types of $TiO_2$ nanoparticles were washed, suspended in ice-cold distilled water (200 μL), and sonicated for 3 min with a 9 s pulse with 1 s off. Then, in order to avoid the influence of fluorescence from $TiO_2$ nanoparticles, all the samples were spinned and only clear supernatant (100 μL) was added to the reaction buffer (1 mL) composed of Amplex red (10 μM), Tris-HCl (10 mM, pH 7.4), and horseradish peroxidase (1 unit $mL^{-1}$), and mixed carefully. The mixture was transferred into a 96-well dish and incubated at 37 °C for 5 min before the fluorescence measurement. Fluorescence of the reaction buffer and the sample solution was measured with a FLEXstation™ benchtop scanning fluorometer (Molecular Devices) with excitation and emission at 560 and 590 nm, respectively.

## Acknowledgements

*Financial support by National Science Foundation MRSEC program is gratefully acknowledged.*

  

[1] P. Ball, *Nature* **2001**, *414*, 142.
[2] a) L. L. Muldoon, M. Sandor, K. E. Pinkston, E. A. Neuwelt, *Neurosurgery* **2005**, *57*, 785; b) T. Neuberger, B. Schopf, H. Hofmann, M. Hofmann, B. von Rechenberg, *J. Magn. Magn. Mater.* **2005**, *293*, 483; c) J. Kreuter, *J. Controlled Release* **1991**, *16*, 169; d) S. Jin, K. M. Ye, *Biotechnol. Prog.* **2007**, *23*, 32; e) N. C. Bellocq, S. H. Pun, G. S. Jensen, M. E. Davis, *Bioconjugate Chem.* **2003**, *14*, 1122; f) J. C. Riboh, A. J. Haes, A. D. McFarland, C. R. Yonzon, R. P. Van Duyne, *J. Phys. Chem. B* **2003**, *107*, 1772; g) J. F. Kukowska-Latallo, K. A. Candido, Z. Y. Cao, S. S. Nigavekar, I. J. Majoros, T. P. Thomas, L. P. Balogh, M. K. Khan, J. R. Baker, *Cancer Res.* **2005**, *65*, 5317.
[3] a) V. L. Colvin, *Nat. Biotechnol.* **2003**, *21*, 1166; b) E. Oberdorster, *Environ. Health Perspect.* **2004**, *112*, 1058; c) S. Foley, C. Crowley, M. Smaihi, C. Bonfils, B. F. Erlanger, P. Seta, C. Larroque, *Biochem. Biophys. Res. Commun.* **2002**, *294*, 116.
[4] Y. Pan, S. Neuss, A. Leifert, M. Fischler, F. Wen, U. Simon, G. Schmid, W. Brandau, W. Jahnen-Dechent, *Small* **2007**, *3*, 1941.
[5] N. Pernodet, X. H. Fang, Y. Sun, A. Bakhtina, A. Ramakrishnan, J. Sokolov, A. Ulman, M. Rafailovich, *Small* **2006**, *2*, 766.
[6] V. L. Colvin, *Nat. Biotechnol.* **2003**, *21*, 1166.
[7] a) B. K. Bernard, M. R. Osheroff, A. Hofmann, J. H. Mennear, *J. Toxicol. Environ. Health* **1990**, *29*, 417; b) J. L. Chen, W. E. Fayerweather, *J. Occup. Environ. Med.* **1988**, *30*, 937; c) G. A. Hart, T. W. Hesterberg, *J. Occup. Environ. Med.* **1998**, *40*, 29.
[8] M. Cho, H. Chung, W. Choi, J. Yoon, *Water Res.* **2004**, *38*, 1069.
[9] O. Carp, C. L. Huisman, A. Reller, *Prog. Solid State Chem.* **2004**, *32*, 33.
[10] R. Dunford, A. Salinaro, L. Z. Cai, N. Serpone, S. Horikoshi, H. Hidaka, J. Knowland, *FEBS Lett.* **1997**, *418*, 87.
[11] T. C. Long, J. Tajuba, P. Sama, N. Saleh, C. Swartz, J. Parker, S. Hester, G. V. Lowry, B. Veronesi, *Environ. Health Perspect.* **2007**, *115*, 1631.
[12] a) E. M. Ophus, L. Rode, B. Gylseth, D. G. Nicholson, K. Saeed, *Scand. J. Work Environ. Health* **1979**, *5*, 290; b) R. C. Lindenschmidt, K. E. Driscoll, M. A. Perkins, J. M. Higgins, J. K. Maurer, K. A. Belfiore, *Toxicol. Appl. Pharmacol.* **1990**, *102*, 268; c) G. Oberdorster, J. Ferin, B. E. Lehnert, *Environ. Health Perspect.* **1994**, *102*, 173.
[13] C. M. Sayes, R. Wahi, P. A. Kurian, Y. P. Liu, J. L. West, K. D. Ausman, D. B. Warheit, V. L. Colvin, *Toxicol. Sci.* **2006**, *92*, 174.
[14] J. R. Gurr, A. S. S. Wang, C. H. Chen, K. Y. Jan, *Toxicology* **2005**, *213*, 66.
[15] W. A. Lee, N. Pernodet, B. Q. Li, C. H. Lin, E. Hatchwell, M. H. Rafailovich, *Chem. Commun.* **2007**, 4815.
[16] K. Ghosh, Z. Pan, E. Guan, S. R. Ge, Y. J. Liu, T. Nakamura, X. D. Ren, M. Rafailovich, R. A. F. Clark, *Biomaterials* **2007**, *28*, 671.
[17] K. Ghosh, X. D. Ren, X. Z. Shu, G. D. Prestwich, R. A. F. Clark, *Tissue Eng.* **2006**, *12*, 601.
[18] H. Hidaka, S. Horikoshi, N. Serpone, J. Knowland, *J. Photochem. Photobiol. A* **1997**, *111*, 205.
[19] J. P. Eu, L. M. Liu, M. Zeng, J. S. Stamler, *Biochemistry* **2000**, *39*, 1040.

Received: June 6, 2008
Revised: October 14, 2008

  